ARTICLE

Steric and Electronic Effects of Ligand Substitution on Redox-Active Fe_4S_4-Based Coordination Polymers

Omar Salinas[#], Jiaze Xie[#], Robert J. Papoular, Noah E. Horwitz, Erik Elkaim, Alexander S. Filatov, John S. Anderson*

One of the notable advantages of molecular materials is the ability to precisely tune structure, properties, and function via molecular substitutions. While many studies have demonstrated this principle with classic carboxylate-based coordination polymers, there are comparatively fewer examples where systematic changes to sulfur-based coordination polymers have been investigated. Here we present such a study on 1D coordination chains of redox-active Fe_4S_4 clusters linked by methylated 1,4-benzene-dithiolates. A series of new Fe_4S_4-based coordination polymers were synthesized with either 2,5-dimethyl-1,4-benzenedithiol (DMBDT) or 2,3,5,6-tetramethyl-1,4-benzenedithiol. The structures of these compounds have been characterized based on synchrotron X-ray powder diffraction while their chemical and physical properties have been characterized by techniques including X-ray photoelectron spectroscopy, cyclic voltammetry and UV–visible spectroscopy. Methylation results in the general trend of increasing electron-richness in the series, but the tetramethyl version exhibits unexpected properties arising from steric constraints. All these results highlight how substitutions on organic linkers can modulate electronic factors to fine-tune the electronic structures of metal-organic materials.

Introduction

Coordination polymers continue to be a research area of growing interest due to their modular nature as well as their applicability in areas including gas separation, storage, catalysis and medicine.[1] A large fraction of coordination polymers rely on oxygen rich nodes or secondary building units (SBUs) with bridging linkers that generally bind through O or N.[2] These design principles enable the synthesis of a broad array of materials, and in many cases the functionality of these materials can be tuned by molecular modifications to the organic linkers.[3] Indeed, this synthetic modularity is one of the key strengths of coordination polymer materials.

Despite the vast array and immense success of O- or N-based coordination polymers, moving to materials composed of heavier elements, particularly S, is attractive for many applications, particularly ones which require a high degree of covalency or electronic coupling.[4] There are several examples where S-based coordination polymers exhibit exceptional properties, but materials composed of metal-heavy chalcogenide clusters and S-based ligands are still comparatively understudied.[5] The dramatically different synthetic procedures, M-S bond strengths, and stabilities of sulfur-rich coordination polymers raise the question of whether the molecular tunability that is a hallmark of classic coordination polymers is preserved with heavier chalcogenide analogues.

Iron-sulfur clusters, which are key cofactors in biology,[6] are particularly appealing candidates for MOF nodes. Despite this, there have been relatively few examples of materials designed around these units.[7] Previously, our group demonstrated that one of the most thoroughly studied molecular sulfide clusters, Fe_4S_4 clusters, can be linked with 1,4-benzenditiolate (BDT) through solvothermal reactions to generate charged highly crystalline 1D-chain polymers.[8] The physical properties of these materials can be tuned via cluster-based redox events and are also sensitive to the choice of counterions. The comparatively simple composition and structure of these materials prompted us to examine whether molecular tuning of the dithiolate linker to modulate physical properties would be possible.

Herein, we report new Fe_4S_4-based chains synthesized using two methylated linker variants, 2,5-dimethyl-1,4-benzenedithiol (DMBDT) and 2,3,5,6-tetramethyl-1,4-benzenedithiol (TMBDT). The dimethylated compound $[Fe_4S_4(DMBDT)_2][TBA]_2$ (TBA = NBu_4^+) was generated with the DMBDT ligand and TBA cations (**1**, Scheme 1). Two permethylated compounds, $[Fe_4S_4(TMBDT)_2][TEA][Li]$ (TEA = NEt_4^+, **2**) and $[Fe_4S_4(TMBDT)_2][TBA]_x[Li]_{2-x}$ (**3**), were made with the TMBDT ligand using either TEA or TBA cations. X-ray powder diffraction (XRPD) data were collected on this group of materials, and the structure of **1** was elucidated via rigorous and detailed *ab initio* structure solution and Rietveld refinement based on synchrotron XRPD data. Cyclic voltammetry (CV) reveals the redox activity of the Fe_4S_4 clusters is maintained, and shows that the degree of methylation of the linker influences the redox potential of these polymers. These results

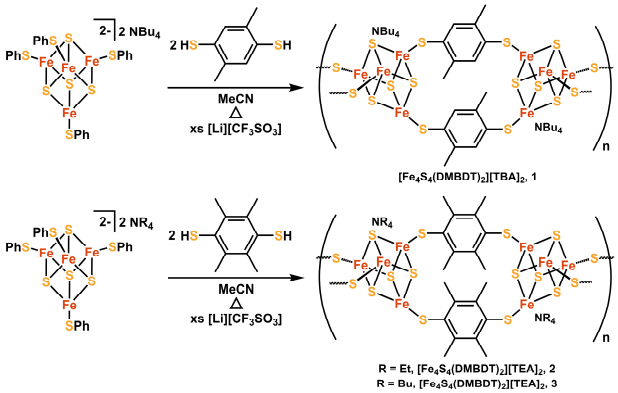

Scheme 1. Synthesis of Fe_4S_4 chain compounds **1**-**3** with differentially methylated 1,4-benzenedithiol ligands.

demonstrate that iron-sulfur cluster-based coordination polymers can be tuned by linker functionalization, but that permethylation results in additional changes to packing and properties. This study shows that the properties of S-based coordination polymers can be tuned in an analogous manner to that observed in MOFs supporting that the molecular design principles that are a strength of coordination polymers are also applicable in heavier chalcogenide analogues.

Results and Discussion

Synthesis and Composition of Coordination Polymers

Solvothermal reaction conditions similar to those previously reported were followed and modified to obtain the desired materials (Scheme 1).[8] In the case of **1**, $[Fe_4S_4(SPh)_4][TBA]_2$ was heated with 5 equivalents of DMBDT in acetonitrile (MeCN) resulting in the formation of a dark purple solid. Similarly, the syntheses of **2** and **3** were performed by heating Fe_4S_4 precursors with the appropriate cation with 2 equivalents of TMBDT in MeCN. Consistent with our previous report, the addition of excess $[Li][CF_3SO_3]$ was used to increase crystallinity. During optimization of the synthesis conditions, we also noted that the yield of **3** was increased with the addition of $[TBA][PF_6]$. The influence of these additives underscores the importance that ion concentrations have in the packing and crystallinity of these charged 1D structures.

After isolating **1**-**3** as solids we then performed several experiments to examine the chemical composition of these materials. Digestion of **1**-**3** in 12 M hydrochloric acid followed by extraction in CD_2Cl_2 or C_6D_6 and ^1H NMR analysis confirmed the incorporation of the methylated ligands in the structures (Figure S7, S9, and S11). The complete substitution of the thiophenolate ligands was further established by Infrared spectroscopy (IR) which shows that no thiophenol (-SH) stretches are observed which would be present if residual protonated linkers were present (Figure S15-S17). This is also confirmed by the absence of thiophenol features in the digestion experiments. Alternatively, digestion in D_2SO_4 diluted with DMSO-d_6 followed by ^1H NMR analysis confirms the incorporation of the counterions, TEA and TBA, in all three corresponding materials (Figure S8, S10, and S12).

X-ray fluorescence (XRF) and X-ray photoelectron spectroscopy (XPS) data were also collected on **1**-**3** to further corroborate the assigned compositions and ascertain any differences arising from methylation of the linkers. XRF analysis shows Fe:S ratios of 0.5 for **1**, **2**, and **3**, consistent with the expectation of two S-based linkers per Fe_4S_4 cluster (See Table S1). However, while the Fe:S ratio is similar to the previously synthesized unmethylated materials by XRF, XPS data shows a higher than expected Fe:N ratio for the TMBDT materials. In addition, Inductively-Coupled Plasma Mass Spectrometry and Optical Emission Spectroscopy (ICP-MS and ICP-OES) data also shows a significant amount of Li in these materials. These data suggest that the cation composition in the TMBDT materials may be different with some Li^+ replacing the alkyl ammonium cations.

Elemental analysis confirms a more complicated composition for the TMBDT materials. Compound **1** passes combustion analysis for the formula $[Fe_4S_4(DMBDT)_2][TBA]_2$. Conversely, combustion analysis on **2** is more consistent with a formula of $[Fe_4S_4(TMBDT)_2][TEA][Li]$. Notably, this composition is also consistent with both XPS and ICP-MS analysis. We have been unable to obtain combustion analysis on **3** which is consistent with a simple formula and thus we propose the ambiguous formula $[Fe_4S_4(TMBDT)_2][TBA]_x[Li]_{2-x}$. ICP-OES and XPS data on **3** support a comparatively higher Li content (x ~ 1.3), and we suspect that variable cations and solvation may make the exact composition of this compound somewhat ill-defined. Nevertheless, the XRF analysis and structural analysis (see below) supports a chain structure in this material as well.

The sum of these composition analyses suggests that the cluster to linker ratio of these materials can be preserved with methylation of the dithiolate linker, but that permethylation of the benzenedithiolate linker results in a different preferential composition, likely as a result from steric constraints on packing between the comparatively bulky methyl groups with large alkyl ammonium cations.

Structural Data and Crystal Structure Solution of Compound 1

The impact of the methyl groups on the packing of compounds **2** and **3** can also be inferred from the crystallinity of these compounds compared with the previous materials $[Fe_4S_4(BDT)_2][NR_4]_2$ as well as **1**. While compound **1** is highly crystalline (see below), similar to the BDT based compounds, both **2** and **3** have limited or no crystallinity. This makes confidently assigning the structure of these materials challenging. While the compositional data supports the possibility of a chain structure, we also worked to obtain structural data to support this assignment. As such, SAXS data were acquired on **3** (Figure S26). Fitting the data provides a power-law slope of −2. Notably, the previous chain materials with BDT show a −5/3 power law. The larger value observed in **3** could in principle be due to the formation of a 2D sheet, but it could also arise from an expanded swollen coil.[9] Such an expanded swollen coil would be expected if the steric requirements of the linker were larger, precisely as is the case in **3**. As such, SAXS data support a similar chain structure in the TMBDT materials even though we do not have an atomically

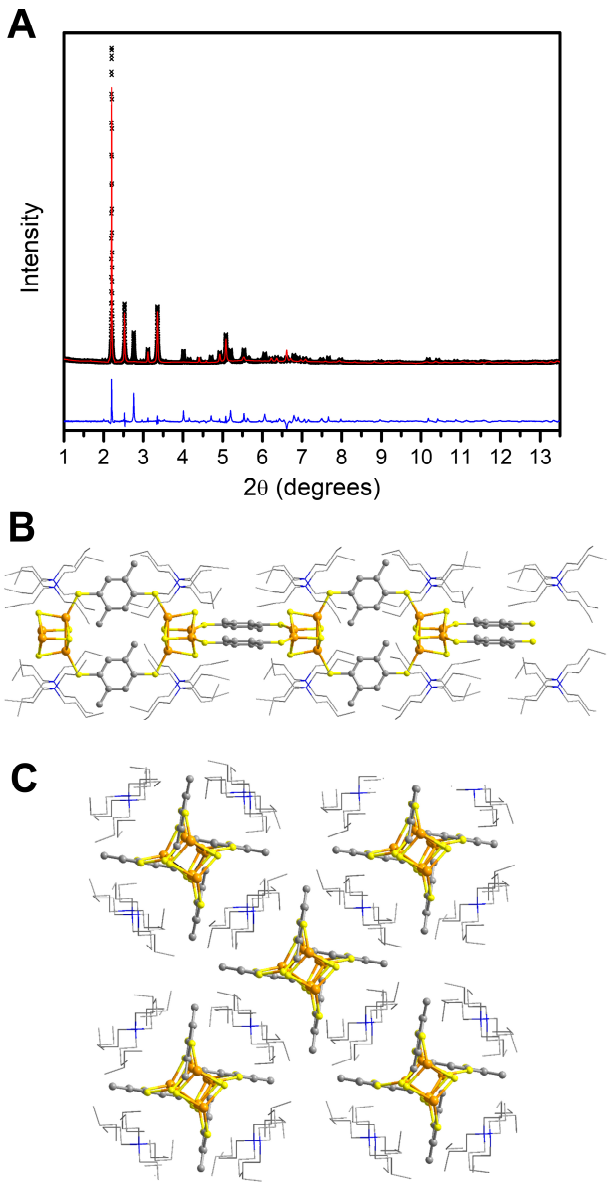

Figure 1. Structural determination of compound **1**. (A) XRPD pattern (black) with Rietveld fit (red) and residual (blue). (B) Side view of chains with a ball-and-stick model. (C) End view of chains.

resolved structure for these compounds due to the poor crystalline packing induced by the permethylation of the linkers. In contrast, the dimethylated material **1** is highly crystalline enabling structure solution from powder data (Figure 1A).[10] The crystal structure of **1** was solved *ab initio* using chemical crystallographic knowledge from the compound with unmethylated BDT ligands, simulating annealing, and then refined with the Rietveld method from high-resolution (HR) synchrotron XRPD data (Figure 1). The X-ray data were first collected at the CRISTAL HR XRPD beamline of the SOLEIL synchrotron [*l* = 0.72800 Å] on a first sample (Figure S21), and then at the 11-BM HR beamline [λ = 0.45793 Å] of the APS synchrotron on a second subsequently synthesized purer sample. The indexing process (using PREDICT/DICVOL) carried out independently on the data collected at both synchrotrons revealed a tetragonal unit cell with a very large volume of about 12000 Å, approximately four times larger than the tetragonal unit cell of $[Fe_4S_4(BDT)_2][TBA]_2$ (a' = 2a , c' = c).[11] This substantially complicated the solution of this structure, but via a careful analysis a successful solution was obtained.

We initially assumed, based on our previous compounds, that the structure consisted of $Fe_4S_4(DMBDT)_2$ chains running along the *c*-axis, with TBA cations located at about the mid-distance between the Fe_4S_4 clusters and neighboring chains. The unit cell content as well as the symmetry of the two distinct moieties in **1** puts a limit on the overall symmetry of the unit cell, thus restricting Z to a maximum value of 8 and yielding a large volume of about 1500 Å for the asymmetric unit.

A high symmetry space group $P4_2/ncm$ (#138) with Z = 16 accounts for all of the X-ray 11-BM data reflections and absences, whereas the CRISTAL data were marred with a few weak impurity lines. As the polymeric $Fe_4S_4(DMBDT)_2$ chains are incompatible with diagonal mirror symmetry, the $P4_2/n$ (#86) with Z = 8 tetragonal space group, which is a maximal subspace group of $P4_2/ncm$, was chosen instead. The validity of a chemically sensible packing of the components of **1** using the $P4_2/n$ space group was established using FOX simulations with Simulated Annealing and Rigid Bodies.[12] As mentioned, the large volume of the unit cell and the large number of independent atoms (150) in **1** presents a significant challenge for structure solution. To alleviate this issue, we started with the most symmetric models that involve the smallest number of free parameters.

In the present case, the crystal structure comprises two distinct building blocks of $Fe_4S_4(DMBDT)_2$ and TBA. The initial Fe_4S_4 cluster was modeled using literature-based bond lengths of Fe–S = 2.272 Å and Fe–Fe = 2.735 Å in the cuboidal core which yields a S–S distance of 3.610 Å if one assumes perfectly regular S and Fe tetrahedra in the cluster.[13] For the DMBDT molecules, the C–C bond lengths were taken as 1.4 Å, 1.506 Å for the C–S bonds, and 1.0 Å for the C–H bonds. The TBA molecule was built using C–N and C–C bond lengths both equal to 1.51 Å, as well as a C–H bond distance of 1.0 Å.

The model of the polymeric $Fe_4S_4(DMBDT)_2$ chain was built using the previously reported structure of $[Fe_4S_4(BDT)_2][TBA]_2$.[8] To reduce the number of variables, an initial starting extended model was built with coplanar DMBDT rings to make them related through an inversion center. Further distortion of the 1D chain is carried out to maintain the maximum symmetry to allow chemically sensible H···H interatomic distances. This procedure results in a rotation of the two DMBDT sides by 19° with respect to the main chain. For further details on the structural manipulations and the Python code written to perform them, see the ESI. The rotation of the independent DMBDT rings requires that the whole 1D polymeric chain be counter-rotated by 8° in order to leave as much space as possible for the TBA cations. Alternative rotations of the chains and ligands were also considered but were rejected based on the quality of their Rietveld refinements (See the ESI).

For symmetry reasons, the N atoms of the TBA cations were placed at midpoints between the centers of neighboring Fe_4S_4

clusters. This choice leads to the (0 1/4 1/4) and (0 3/4 1/4) independent positions in the unit cell. The positioning of the whole TBA cations (in spite of a deceptive two-fold indetermination) was chosen unequivocally to produce the largest S···C interatomic contacts resulting in a good agreement with the associated van der Waals distance (3.5 Å). The outer -CH_2-CH_3 tails of the butyl substituents were also adjusted in compliance with the molecular bond distances and bond angles in order to further minimize a number of other very short interatomic contacts such as C···H and H···H interactions between neighboring TBA cations or TBA cations and an adjacent polymeric chain.

The obtained model was then 'frozen' and used for the Rietveld refinement using the GSAS software package producing a final Rp value of approximately 15% (Figure 1A).[14] Further Rietveld refinement attempts using numerous alternative and often conflicting structural restraints led to unsolvable problems with respect to the least-squares convergence. While the rigid-body approach is certainly an acceptable structure solution in this case, a less than ideal fit (which is typically considered to be less than 15% for the Rp factor of merit) is obtained due to the need to use a higher symmetry than is likely for the molecular subunits in order to describe this large crystal structure (1200 atoms in the unit cell). With this in mind, only the intermolecular contacts and general packing can be reliably interpreted.

The crystal structure of **1** consists of chains of Fe_4S_4 clusters connected by pairs of DMBDT groups surrounded by TBA cations. Another way to look at the suggested crystal structure is in terms of TBA-built tubes or TBA-sheaths surrounding each 1D $Fe_4S_4(DMBDT)_2$ polymeric chain (Figure 1B and C and Figure S25). This is overall similar to the previously reported complex $[Fe_4S_4(BDT)_2][TBA]_2$.[8] The separation between Fe_4S_4 clusters within the polymeric chains is now 10.38 Å, which is slightly more than the previously observed value of 9.92 Å. This expanded value is consistent with the larger steric constraints imposed by the methylation of the linker. Furthermore, while the sheathed structure of **1** is similar to that observed in $[Fe_4S_4(BDT)_2][TBA]_2$ the overall packing of the chains and countercations is quite different, as is clearly illustrated by an end-on view of the structure (Figure 1C).

Overall, this challenging structural analysis verifies that the chain structure of these compounds is preserved in **1**. Furthermore, the packing and inter-cluster distances observed in **1** support that the steric constraints of the organic linker, even with the substitution of two comparatively small methyl groups, can have a large perturbative effect on the structure. This is consistent with the poorer crystallinity and alternative cation incorporation observed in **2** and **3**. With a firmer picture of the structural ramifications of linker methylation we then turned to examining what electronic effects this substitution had.

Electronic Properties of Coordination Polymers

UV-visible spectroscopy (UV-vis) was initially employed to investigate the electronic properties of **1** and **3** (Figure 2).

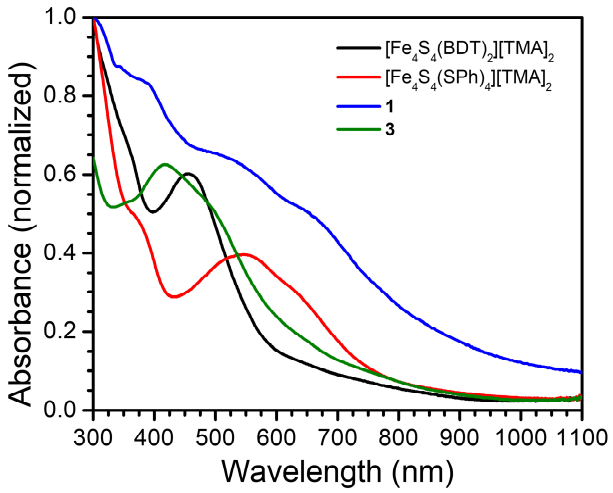

Figure 2. Normalized UV-visible spectra of **1**, **3**, and reference compounds in DMF solution.

Unfortunately, **2** was insoluble in all solvents we examined, precluding more detailed characterization of its properties. In our previous work we used shifts in features at around 450 nm from the monomeric clusters, assigned as ligand-to-metal charge transfer transitions, as markers for how electron-rich the chains were. Given this hypothesis, we expected to observe more significant red-shifts in the methylated materials arising from an increased inductive donation. A shift in comparison to monomeric iron-sulfur clusters is observed as expected, however, a comparison to the unmethylated BDT derivative is convoluted by broadening and splitting of the features. Nevertheless, there appears to be little to no shift in the energies of the features between **1** and $[Fe_4S_4(BDT)_2][TMA]_2$ with the main features in **1** coming at ~530 and ~660 nm. Furthermore, compound **3** doesn't show similarly red-shifted features, but instead shows one blue shifted feature at ~420 nm and another shoulder at ~500 nm when compared with $[Fe_4S_4BDT_2][[TMA]_2$ and the monomeric thiophenolate capped cluster.

These results are inconsistent with our initial hypothesis, but are actually expected based on prior literature studies on the effect of methylation of thiophenolate donors on Fe_4S_4 clusters.[15] The enhanced steric requirements imposed by methylation can influence both the Fe–S distance as well as the Fe–S–C angle, causing differential red- or blue-shifts based on different donation from S as a result of these structural changes. Indeed, the structure of **1** shows different orientations of the linker due to methylation, supporting this conclusion. We propose that there is competition between enhanced donation from the methyl groups and steric constraints in **1**, resulting in no significant shift from the features in $[Fe_4S_4BDT_2][TMA]_2$, but that steric effects dominate in **3** resulting in the observed blue-shift.

We also performed electrochemical analysis to further investigate how methylation affects the electronic structure of these chains. Two iron-sulfur cluster reductive features were observed previously, corresponding to the $[Fe_4S_4]^{2+}/[Fe_4S_4]^{+}$ and

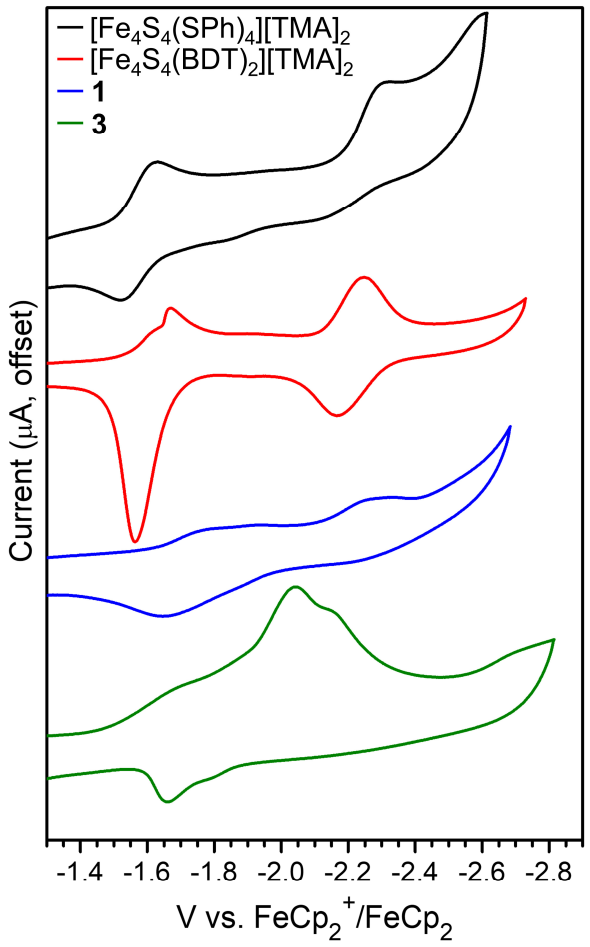

Figure 3. Cyclic voltammograms of **1**, **3**, unmethylated $[Fe_4S_4(BDT)_2][TMA]_2$, and monomeric $[Fe_4S_4(SPh)_4][TMA]_2$. Conditions: DMF, 0.2 M $[Li][CF_3SO_3]$, 0.1 V/s.

$[Fe_4S_4]^+/[Fe_4S_4]^0$ couples. As before, the redox activity of **1** and **3** was examined by cyclic voltammetry in a solution of Dimethylformamide (DMF) with $[Li][CF_3SO_3]$ as the electrolyte (Figure 3). The reductive features for the unmethylated material were observed at −1.6 and −2.2 V vs $FeCp_2^+/FeCp_2$. Slight shifts to more negative potentials are observed for **1**, with similar features observed at −1.8 and −2.3 V vs $FeCp_2^+/FeCp_2$, confirming the hypothesis that more electron-donating methyl-substituted linkers results in more electron-rich chains. These results also demonstrate that the redox activity of the Fe_4S_4 clusters is preserved even with methylation on the ligand. The first reductive feature, assigned as the $[Fe_4S_4]^{2+}/[Fe_4S_4]^+$ couple is reversible upon cycling but the second feature is only quasi-reversible (Figure S18).

While the voltammogram of **1** displays a similar pattern to that of $[Fe_4S_4(BDT)_2][[TMA]_2$, the voltammogram of **3** is significantly different. The first reductive feature of **3** shifts to more negative potentials but the second reductive feature shifts to more positive potentials. This observation is consistent with the UV-vis data suggesting that the steric constraints in **3** lead to a more complicated effect on electronic structure than would be expected from a simple enhancement of donation from methylation. Finally, we also collected electrical conductivity data for **1**-**3** which were generally consistent with the unmethylated material (See Table S2). This is consistent with the hypothesis that bulk electrical conductivity is more limited by the insulating alkylammonium cations than the inherent electronic structure of the chains.

Conclusions

In this work we have examined how linker methylation affects the physical properties of coordination polymer chains composed of Fe_4S_4 clusters. Solvothermal synthesis enabled the generation of three new chain materials. The structure of the dimethylated DMBDT variant **1** was determined by *ab initio* structure solution and Rietveld refinement. Further methylation, however, led to Li incorporation and more complicated structures, compositions, and solubility. The electronic structures of these new materials were investigated by UV-vis spectroscopy and electrochemistry. These analyses show parallels between how methylation affects the electronic structure of molecular and extended materials composed of Fe_4S_4 clusters. Overall, this work describes a systematic approach in exploring the effects of methylation on the ligand component of S-based coordination polymers. Importantly, the molecular design principles that make coordination polymers attractive classes of materials for many applications are preserved in heavier chalcogenide analogues, paving the way to expanding families of these promising materials.

Experimental Section

All manipulations were performed under an inert atmosphere of dry nitrogen gas using a Schlenk line or N_2-filled MBraun UNILab glovebox unless otherwise noted. ^1H NMR measurements were performed on Bruker DRX 400 or 500 spectrometers. Elemental analyses (C, H, N) were performed by Midwest Microlabs. Dimethylformamide (DMF) and acetonitrile (MeCN) were initially dried and purged with N_2 on a solvent purification system from Pure Process Technology. DMF and MeCN were then passed through activated alumina and stored over 4Å molecular sieves. Dimethylacetamide (DMA) was sparged with N_2, transferred into the glovebox, passed through activated alumina and stored over 4Å molecular sieves. $[TBA][PF_6]$ was recrystallized from H_2O and dried at 160 °C before use. $[Fe_4S_4(SPh)_4][TEA]_2$, $[Fe_4S_4(SPh)_4][TBA]_2$ were prepared as previously described. [16] 1,4-dibromo-tetramethylbenzene was prepared following literature procedure. [17] The synthesis of 1,4-bis(isopropylthio)-2,3,5,6-tetramethylbenzene and 1,4-bis(isopropylthio)-2,5-dimethylbenzene were performed via modification of a related synthesis.[8] 2,5-dimethyl-1,4-benzenedithiol and 2,3,5,6-tetramethyl-1,4-benzenedithiol have been previously reported,[18] but were synthesized using an alternate procedure as shown below.[8] All synthesis of **1**-**3** were conducted in a N_2-

filled glovebox. All other chemicals were purchased through commercial means unless noted.

1,4-Bis(isopropylthio)-2,5-dimethylbenzene. A dispersion of 60% NaH in mineral oil (6.4 g, 160 mmol) was added to a 500 mL three-neck flask and then washed with hexane twice and dimethylacetamide (DMA) once under a N_2 atmosphere. After adding DMA (33 mL), 2-propanethiol (17.3 mL, 160 mmol) was injected slowly and in portions to avoid excessive foaming (if necessary, use of an ice bath and drop funnel is helpful). Subsequently, DMA (33 mL) and a solution of 2,5-dimethyl-1,4-dibromobenzene (10.56 g. 40 mmol) in DMA (50 mL) were injected, and the mixture was heated for 17 h to 100 °C. The mixture was cooled, poured into 33 mL saturated NaCl solution and extracted with Et_2O (3 × 33 mL). The organic layer was washed with H_2O (5 × 50 mL), dried with [Mg][SO_4], and evaporated. The yellowish solid was further purified by vacuum distillation. Yield: 9.9 g (97%).^{1}H NMR (400 MHz, $CDCl_3$) δ 7.19 (1 H, s), 3.33 (2 H, spt, J = 8.0 Hz), 2.35 (12 H, s), 1.30 (12 H, d, J = 4 Hz) ppm. ^{13}C NMR (400 MHz, $CDCl_3$) δ 20.36, 23.25, 37.81, 133.21, 133.27, 137.24. Anal. Calc. for $C_{14}H_{22}S_2$: C 66.09%, H 8.72%. Found: C 66.24%, H 8.84%.

2,5-dimethyl-1,4-benzenedithiol. Sodium (4.0 g, 180 mmol), dry DMA (100 mL) from the glovebox, and 1,4-Bis(isopropylthio)benzene (4.5 g, 18 mmol) were added in sequence to a 250 mL three-necked flask under N_2 atmosphere and the mixture was heated to 100 °C for 8 h. During this time the reaction mixture became yellow with thick precipitate. The reaction solution was quenched with diluted HCl solution (concentrated HCl solution (34−37% w/w, 20 mL) + H_2O (105 mL)) in an ice bath and stirred for another 0.5 h under an inert atmosphere. The mixture was then extracted with Et_2O (2 × 75 mL). The organic layer was washed with H_2O (5 × 30 mL), dried with [Mg][SO_4], and evaporated. A white powder was obtained by washing with hexanes (20 mL). More product can be recovered by storing the hexane washes in a freezer (−35 °C) overnight, resulting in a pale yellow powder. Overall yield: 2.4 g (80%). ^{1}H NMR (400 MHz, $CDCl_3$) δ 7.09 (2 H, s), 3.20 (2 H, s), 2.25 (2 H, s) ppm. Other spectroscopic characterization was identical to that previously reported.[18a]

1,4-bis(isopropylthio)-2,3,5,6-tetramethylbenzene. A dispersion of 60% NaH in mineral oil (6.4 g, 160 mmol) was added to a 500 mL three-neck flask and then washed with hexane twice and DMA once under a N_2 atmosphere. After adding DMA (40 mL), 2-propanethiol (17.4 mL, 160 mmol) was injected slowly and in portions to avoid excessive foaming. Subsequently, DMA (40 mL) and a solution of 1,4-dibromo-tetramethylbenzene in DMA (40 mL) were injected, and the mixture was heated for 17 h to 100 °C. The mixture was cooled, poured into 40 mL saturated brine solution and extracted with Et_2O (3 × 50 mL). The organic layer was washed with H_2O (4 × 30 mL), dried with [Mg][SO_4] and evaporated. The final product was white powders. Yield: 11.5 g (99%). ^{1}H NMR (400 MHz, $CDCl_3$) δ 3.01 (2 H, spt, J = 3.0 Hz), 2.58 (12 H, s), 1.18 (12 H, d, J = 1.2 Hz) ppm. ^{13}C NMR (400 MHz, $CDCl_3$) δ 20.56, 23.25, 39.69, 134.84, 139.47. Anal. Calc. for $C_{16}H_{26}S_2$: C 68.03%, H 9.28%. Found: C 68.85%, H 9.51%.

2,3,5,6-tetramethyl-1,4-benzenedithiol. Sodium (1.8 g, 80 mmol), dry DMA (40 mL) from the glovebox, and 1,4-bis(isopropylthio)-2,3,5,6-tetramethylbenzene (5.6 g, 20 mmol) were added in sequence to a 125 mL three-neck flask under N_2 atmosphere and the mixture was heated to 100 C for 8h. The reaction solution was quenched with diluted HCl (concentrated HCl solution (34-37% w/w, 10 mL) + H_2O (50 mL)) in an ice bath and stirred for another 0.5 h under an inert atmosphere. The mixture was extracted with Et_2O (3 × 50 mL). The organic layer was then washed with H_2O (5 × 30 mL), dried with [Mg][SO_4] and evaporated. A white powder was obtained by washing with cold hexanes (20 mL) and dried. The product was stored in the glovebox for the usage. Yield: 2.7 g (69%). ^{1}H NMR (400 MHz, $CDCl_3$) δ 3.19 (2 H, s), 2.40 (12 H, s) ppm. Other spectroscopic characterization was identical to that previously reported.[18b]

[Fe_4S_4(DMBDT)$_2$][TBA]$_2$ (1). [Fe_4S_4(SPh)$_4$][TBA]$_2$ (190 mg, 0.15 mmol) and [Li][CF_3SO_3] (117 mg, 0.75 mmol) were added to a 24 mL vial and dissolved in MeCN (4 mL). A solution of 2,5-dimethyl-1,4- benzenedithiol (130 mg, 0.75 mmol) in MeCN (3 mL) was added and the vial was sealed and placed in a heating block on a 100 °C hot plate. The reaction mixture was heated for 2 days and the solid was separated by centrifugation, washed with MeCN (4 × 4 mL), and dried under vacuum. A dark-purple solid was obtained (53 mg, 30%). Anal. Calc. for $Fe_4S_8C_{48}H_{88}N_2$: C 49.15%, H 7.56%, N 2.39%. Found: C 49.98%, H 7.44%, N 2.55%.

[Fe_4S_4(TMBDT)$_2$][TEA][Li] (2). [Fe_4S_4(SPh)$_4$][TEA]$_2$ (105 mg, 0.10 mmol) and [Li][CF_3SO_3] (300 mg, 2.0 mmol) were added to a 24 mL vial and dissolved in MeCN (6 mL). A solution of 2,3,5,6-tetramethyl-1,4- benzenedithiol (40 mg, 0.20 mmol) in MeCN (4 mL) was added and the vial was sealed and placed in a heating block on a 100 °C hot plate. The reaction mixture was heated for 2 days and further separated by centrifugation, washed with MeCN (4 × 4 mL), and dried under vacuum. A dark-brown solid was obtained (46 mg, 45%). Anal. Calc. for $Fe_4S_8C_{28}H_{44}NLi$: C 38.15%, H 5.03%, N 1.59%. Found: C 36.83%, H 5.38%, N 1.64%.

[Fe_4S_4(TMBDT)$_2$][TBA]$_x$[Li]$_{2-x}$ (3). [Fe_4S_4(SPh)$_4$][TBA]$_2$ (130 mg 0.10 mmol), [Li][CF_3SO_3] (620 mg, 4.0 mmol), and [TBA][PF_6] (38 mg, 0.10 mmol) were added to a 24 mL vial and dissolved in MeCN (6 mL). A solution of 2,3,5,6-tetramethyl-1,4-benzenedithiol (40 mg, 0.20 mmol) in MeCN (4 mL) was added and the vial was sealed and placed in a heating block on a 100 °C hot plate. The reaction mixture was heated for 2 days and further separated by centrifugation, washed with MeCN (4 × 4 mL), and dried under vacuum. A dark-brown solid was obtained (38 mg, 31%). We were unable to obtain a combustion analysis consistent with a simple molecular formula.

Author Contributions

O. S. and J. X. contributed equally to this work.

Conflicts of interest

There are no conflicts to declare.

Acknowledgements

We gratefully acknowledge funding for this work from the National Science Foundation through grant # DMR-2002367. J.S.A. also gratefully acknowledges support from the Sloan Research Foundation (FG-2019-11497) and 3M Corporation through an NTFA. Use of the Advanced Photon Source at Argonne National Laboratory was supported by the U.S. Department of Energy, Office of Science, Office of Basic Energy Sciences, under Contract No. DE-AC02-06CH11357, and we thank the 11-BM beamline staff. SOLEIL Synchrotron beamtime at the CRISTAL beamline is appreciatively acknowledged. Dr. Mrinal Bera is thanked for helpful discussions of SAXS data, Professor Dmitri Talapin and his group are thanked for assistance with ICP-OES data acquisition, and Professor Wenbin Lin and his students Xiaomin Jiang and Yingjie Fan are thanked for assistance with ICP-MS data acquisition.

Notes and references

1. a) H. C. Zhou, J. R. Long, and O. M. Yaghi, *Chem. Rev.,* 2012, **112**, 673-674. b) T. Drake, P. F. Ji and W. B. Lin, *Acc. Chem. Res.*, 2018, **51**, 2129-2138. c) B. R. Barnett, M. I. Gonzalez and J. R. Long, *Trends in Chemistry*, 2019, **1**, 159-171. d) R. B. Lin, S. C. Xiang, W. Zhou and B. L. Chen, *Chem*, 2020, **6**, 337-363. e) K. Y. Ni, T. K. Luo, G. T. Nash and W. B. Lin, *Acc. Chem. Res.*, 2020, **53**, 1739-1748. f) Z. Ji, H. Wang, S. Canossa, S. Wuttke and O. M. Yaghi, *Adv. Funct. Mater.*, 2020, **30**, 2000238.

2. a) H. Deng, S. Grunder, K. E. Cordova, C. Valente, H. Furukawa, M. Hmadeh, F. Gandara, A. C. Whalley, Z. Liu, S. Asahina, H. Kazumori, M. O'Keeffe, O. Terasaki, J. F. Stoddart and O. M. Yaghi, *Science*, 2012, **336**, 1018–1023. b) X. Zhang, Z. J. Chen, X. Y. Liu, S. L. Hanna, X. J. Wang, R. Taheri-Ledari, A. Maleki, P. Li and O. K. Farha, *Chem. Soc. Rev.*, 2020, **49**, 7406-7427. c) H. Ghasempour, K. Y. Wang, J. A. Powell, F. ZareKarizi, X. L. Lv, A. Morsali and H. C. Zhou, *Coord. Chem. Rev.*, 2021, **426**.

3. a) O. M. Yaghi, M. O'Keeffe, N. W. Ockwig, H. K. Chae, M. Eddaoudi and J. Kim, *Nature*, 2003, **423**, 705-714. b) X. Kong, H. Deng, F. Yan, J. Kim, J. A. Swisher, B. Smit, O. M. Yaghi and J. A. Reimer, *Science*, 2013, **341**, 882-885. c) W. Lu, Z. Wei, Z.-Y. Gu, T.-F. Liu, J. Park, J. Park, J. Tian, M. Zhang, Q. Zhang, T. Gentle Iii, M. Bosch and H.-C. Zhou, *Chem. Soc. Rev.*, 2014, **43**, 5561-5593. d) T. Islamoglu, S. Goswami, Z. Y. Li, A. J. Howarth, O. K. Farha and J. T. Hupp, *Acc. Chem. Res.*, 2017, **50**, 805-813. e) O. M. Yaghi, *ACS Central Science*, 2019, **5**, 1295-1300.

4. a) L. F. Szczepura, C. P. Galloway, Y. Zheng, P. Han, S. R. Wilson, T. B. Rauchfuss and A. L. Rheingold, *Angew. Chem. Int. Ed.*, 1995, **34**, 1890-1892. b) T. Kambe, R. Sakamoto, K. Hoshiko, K. Takada, M. Miyachi, J. H. Ryu, S. Sasaki, J. Kim, K. Nakazato, M. Takata and H. Nishihara, *J. Am. Chem. Soc.*, 2013, **135**, 2462-2465. c) L. Sun, T. Miyakai, S. Seki and M. Dincă, *J. Am. Chem. Soc.*, 2013, **135**, 8185-8188. d) T. Kambe, R. Sakamoto, T. Kusamoto, T. Pal, N. Fukui, K. Hoshiko, T. Shimojima, Z. F. Wang, T. Hirahara, K. Ishizaka, S. Hasegawa, F. Liu and H. Nishihara, *J. Am. Chem. Soc.*, 2014, **136**, 14357-14360. e) X. Huang, P. Sheng, Z. Tu, F. Zhang, J. Wang, H. Geng, Y. Zou, C.-a. Di, Y. Yi, Y. Sun, W. Xu and D. Zhu, *Nat. Comm.*, 2015, **6**, 7408. L. Sun, C. H. Hendon, M. A. Minier, A. Walsh and M. Dincă, *J. Am. Chem. Soc.*, 2015, **137**, 6164-6167. c) Y. Sun, L. Qiu, L. Tang, H. Geng, H. Wang, F. Zhang, D. Huang, W. Xu, P. Yue, Y.-s. Guan, F. Jiao, Y. Sun, D. Tang, C.-a. Di, Y. Yi and D. Zhu, *Adv. Mater.*, 2016, **28**, 3351-3358. d) A. J. Clough, J. M. Skelton, C. A. Downes, A. A. de la Rosa, J. W. Yoo, A. Walsh, B. C. Melot and S. C. Marinescu, *J. Am. Chem. Soc.*, 2017, **139**, 10863-10867. e) X. Huang, S. Zhang, L. Liu, L. Yu, G. Chen, W. Xu and D. Zhu, *Angew. Chem. Int. Ed.*, 2018, **57**, 146-150. f) R. Dong, P. Han, H. Arora, M. Ballabio, M. Karakus, Z. Zhang, C. Shekhar, P. Adler, P. S. Petkov, A. Erbe, S. C. B. Mannsfeld, C. Felser, T. Heine, M. Bonn, X. Feng and E. Cánovas, *Nat. Mater.*, 2018, **17**, 1027-1032. g) A. J. Clough, N. M. Orchanian, J. M. Skelton, A. J. Neer, S. A. Howard, C. A. Downes, L. F. J. Piper, A. Walsh, B. C. Melot and S. C. Marinescu, *J. Am. Chem. Soc.*, 2019, **141**, 16323-16330. f) T. Kusamoto and H. Nishihara, *Coord. Chem. Rev.*, 2019, **380**, 419–439. h) Q. Zeng, L. Wang, Y. Huang, S.-L. Zheng, Y. He, J. He, W.-M. Liao, G. Xu, M. Zeller and Z. Xu, *Chem. Commun.*, 2020, **56**, 3645-3648.

5. a) Z. Ji, C. Trickett, X. Pei and O. M. Yaghi, *J. Am. Chem. Soc.*, 2018, **140**, 13618-13622. b) J. Xie, L. Wang, and J. S. Anderson, *Chem. Sci.*, 2020, **11**, 8350–8372. c) J. A. Kephart, C. G. Romero, C.-C. Tseng, K. J. Anderton, M. Yankowitz, W. Kaminsky and A. Velian, *Chem. Sci.*, 2020, **11**, 10744-10751. d) Y. Kamakura and D. Tanaka, *Chem. Lett.*, 2021, **50**, 523-533.

6. a) H. Beinert, R. H. Holm and E. Münck, *Science*, 1997, **277**, 653-659. b) P. Venkateswara Rao and R. H. Holm, *Chem. Rev.*, 2004, **104**, 527-560. c) W. E. Broderick, B. M. Hoffman and J. B. Broderick, *Acc. Chem. Res.*, 2018, **51**, 2611-2619. d) R. D. Britt, G. Rao and L. Tao, *Nature Reviews Chemistry*, 2020, **4**, 542-549. e) Brown, A.C.; Suess, D. L. M.; in *Comprehensive Coordination Chemistry 3* (2021).

7. a) J.-C. Moutet and C. J. Pickett, *J. Chem. Soc., Chem. Commun.*, 1989, **3**, 188-190. b) C. J. Pickett, K. S. Ryder and J.-C. Moutet, *J. Chem. Soc., Chem. Commun.*, 1992, **9**, 694-697. c) C. J. Pickett, K. S. Ryder and J. C. Moutet, *J. Chem. Soc. Dalton*, 1993, **24**, 3695-3703. d) C. J. Pickett and K. S. Ryder, *J. Chem. Soc. Dalton*, 1994, **14**, 2181-2189. e) C. J. Pickett, S. K. Ibrahim and D. L. Hughes, *Faraday Discuss.*, 2000, **116**, 235-244. f) T. P. N., B. Thomas, P. Vasilios and K. M. G., *Angew. Chem. Int. Ed.*, 2000, **39**, 4558-4562. g) B. D. Yuhas, C. Prasittichai, J. T. Hupp and M. G. Kanatzidis, *J. Am. Chem. Soc.*, 2011, **133**, 15854-15857. h) Y. Shim, B. D. Yuhas, S. M. Dyar, A. L. Smeigh, A. P. Douvalis, M. R. Wasielewski and M. G. Kanatzidis, *J. Am. Chem. Soc.*, 2013, **135**, 2330-2337. i) J. Liu, M. S. Kelley, W. Wu, A. Banerjee, A. P. Douvalis, J. Wu, Y. Zhang, G. C. Schatz and M. G. Kanatzidis, *Proc. Natl. Acad. Sci.*, 2016, **113**, 5530-5535. j) Y. Shim, R. M. Young, A. P. Douvalis, S. M. Dyar, B. D. Yuhas, T. Bakas, M. R. Wasielewski and M. G. Kanatzidis, *J. Am. Chem. Soc.*, 2014, **136**, 13371-13380.

8. N. E. Horwitz, J. Xie, A. S. Filatov, R. J. Papoular, W. E. Shepard, D. Z. Zee, M. P. Grahn, C. Glider, and J. S. Anderson, *J. Am. Chem. Soc.,* 2019, **141**, 3940–3951.

9. a) G. Beaucage, *J. Appl. Crystallogr.*, 1995, **28**, 717-728. b) G. Beaucage, *J. Appl. Crystallogr.*, 1996, **29**, 134-146.

10. David, W.I.F., K. Shankland, L.B. McCusker, and C. Bärlocher, eds. *Structure Determination from Powder Diffraction Data*. Oxford: Oxford University Press, **2006**. Oxford Scholarship Online, **2010**. doi: 10.1093/acprof:oso/9780199205530.001.0001.

11. a) D. Louër and A. Boultif, *Powder Diffr.*, 2014, **29**, S7-S12. b) J. R. Blanton, R. J. Papoular and D. Louër, *Powder Diffr.*, 2019, **34**, 233-241.

12. V. Favre-Nicolin and R. Cerny, *J. Appl. Crystallogr.*, 2002, **35**, 734-743.

13. a) L. Que, M. A. Bobrik, J. A. Ibers and R. H. Holm, *J. Am. Chem. Soc.*, 1974, **96**, 4168-4178. b) T. O'Sullivan and M. M. Millar, *J. Am. Chem. Soc.*, 1985, **107**, 4096-4097. c) T. J. Ollerenshaw, C. D. Garner, B. Odell and W. Clegg, *J. Chem. Soc. Dalton*, 1985, **10**, 2161-2165.

14. A.C. Larson and R.B. Von Dreele, "General Structure Analysis System (GSAS)", (Report No. 86-748), Los Alamos National Laboratory, Los Alamos, NM.
15. N. Ueyama, T. Sugawara, M. Fuji, A. Nakamura, and N. Yasuoka, *Chem. Lett.*, 1985, **14**, 175-178.
16. G. Christou, C. D. Garner, A. Balasubramaniam, B. Ridge, H. N. Rydon, E. I. Stiefel,and W. H. Pan. *Inorg. Synth.,* 1982, **21**, 33.
17. I. Kaur, M. Jazdzyk, N. N. Stein, P. Prusevich, and G. P. Miller, *J. Am. Chem. Soc.,* 2010, **132**, 1261-1263.
18. a) P. Beimling and G. Koßmehl, *Chem. Ber.* 1986, **119**, 3198-3203. b) M. S. Raasch, *J. Org. Chem.* 1979, **44**, 2629–2632.